Journal of Applied Physics

RESEARCH ARTICLE | DECEMBER 11 2023

High-temperature efficient luminescence of dilute-nitride InGaAsN quantum dots with deep electron potential

Ayano Morita ; Satoshi Hiura ; Junichi Takayama ; Akihiro Murayama

J. Appl. Phys. 134, 224303 (2023)
https://doi.org/10.1063/5.0173207
CHORUS

Journal of Applied Physics ARTICLE pubs.aip.org/aip/jap

High-temperature efficient luminescence of dilute-nitride InGaAsN quantum dots with deep electron potential

Cite as: J. Appl. Phys. **134**, 224303 (2023); doi: 10.1063/5.0173207
Submitted: 24 September 2023 · Accepted: 22 November 2023 ·
Published Online: 11 December 2023

Ayano Morita, Satoshi Hiura,[a] Junichi Takayama, and Akihiro Murayama

AFFILIATIONS

Faculty of Information Science and Technology, Hokkaido University, Kita 14, Nishi 9, Kita-ku, Sapporo 060-0814, Japan

[a]**Author to whom correspondence should be addressed:** hiura@ist.hokudai.ac.jp

ABSTRACT

The temperature dependence of the optical properties of $In_{0.4}Ga_{0.6}As_{0.98}N_{0.02}$ quantum dots (QDs) was investigated using continuous-wave and time-resolved photoluminescence (PL). Significant increases in the PL peak energy and the PL linewidth were observed at temperatures above 200 K, which reflected the high luminescence efficiency of ground and excited states at high temperatures. The PL decay times of the ground state were almost constant between 200 and 300 K at 200–220 ps, which were significantly longer than that of 38 ps for the $In_{0.4}Ga_{0.6}As$ QDs at 300 K. The temperature independence of the PL decay time represents significant suppression of the thermal escape and the thermal excitation of electrons because the electron ground-state localization energy is much larger than the thermal energy. The PL intensity of the $In_{0.4}Ga_{0.6}As_{0.98}N_{0.02}$ QDs was seven times stronger than that of the $In_{0.4}Ga_{0.6}As$ QDs at 300 K, and this tendency was maintained up to 400 K with a PL intensity one order of magnitude stronger. These findings demonstrate that lowering the QD conduction band by nitrogen incorporation is an effective approach for achieving strong QD luminescence above room temperature.

I. INTRODUCTION

Owing to their highly efficient light emission due to the strong confinement of electrons and holes in a limited space, III–V compound semiconductor quantum dots (QDs) based on InAs or InGaAs materials are expected to be an active layer for future low-power-consumption optical devices.[1] InGaAs QDs have been widely investigated not only for application in lasers[2–5] and infrared photodetectors,[6,7] but also for the understanding of fundamental physics in a single QD, such as Rabi oscillation[8,9] and charge states.[10,11] In general, the optical properties of multilayered InAs QDs degrade due to the accumulation of internal strain originating from the large lattice mismatch with GaAs.[12,13] In addition, the intermixing of In and Ga atoms during the GaAs capping process makes it difficult to control the composition of InAs QDs.[14–16] InGaAs QDs are alternative candidates for multilayered QD structures because of the smaller lattice mismatch with GaAs.[17] Laser diodes based on InGaAs QDs have demonstrated high output power,[18] high optical gain,[19] and low threshold current density.[20,21] However, the luminescence intensity of InGaAs QDs is sufficiently low at room temperature because of the dominant thermal escape of electrons from the QDs.[22,23] This is attributed to the relatively small energy difference between the QD electron states and the GaAs barrier or the wetting layer, which mainly originates from the smaller effective mass of electrons than holes. Therefore, if the thermal escape of electrons is strongly suppressed by increasing the conduction band offset, the decrease in the luminescence intensity with increasing temperature can be suppressed; thus, strong QD luminescence is anticipated above room temperature.

Dilute-nitride III–V semiconductors, such as GaAsN and InGaAsN, are desirable for long-wavelength laser diodes used in optical fiber communications because of their well-known huge bandgap bowing.[24–32] Recently, it has been found that tunnel coupling of the GaAsN quantum well to InAs QDs or InGaAs QDs can achieve highly spin-polarized luminescence of the QDs at and above room temperature.[33,34] Because the incorporation of nitrogen into InGaAs QDs lowers the QD electron states via an increase in the conduction band offset and the electron effective mass, the suppression of the thermal escape of electrons

from the QDs can be expected. However, a nitrogen composition of 0.5%–1% cannot sufficiently suppress the thermal escape of electrons, resulting in weak QD luminescence at high temperatures.[35,36] For InGaAsN QDs with a high nitrogen composition of 4%, the QD luminescence intensity can significantly decrease because of the formation of high-density nonradiative defects.[25,37] Therefore, an appropriate nitrogen composition of InGaAsN QDs is important for achieving efficient QD luminescence above room temperature.

In this study, self-assembled $In_{0.4}Ga_{0.6}As_{0.98}N_{0.02}$ QDs were grown on GaAs to suppress the decrease in the QD luminescence intensity with increasing temperature. The temperature dependence of photoluminescence (PL) emission properties, including PL decay properties, was investigated. We observed significant increases in the PL peak energy and the PL linewidth above 200 K, indicating the high luminescence efficiency of the QD ground and excited states at high temperatures. The PL decay time was almost constant between 200 and 300 K, demonstrating the significant suppression of the thermal escape and the thermal excitation of electrons. Moreover, the PL intensities of the $In_{0.4}Ga_{0.6}As_{0.98}N_{0.02}$ QDs at 300 and 400 K were seven to ten times stronger than those of the $In_{0.4}Ga_{0.6}As$ QDs, respectively.

II. EXPERIMENTAL SECTION

Figure 1(a) shows a schematic of the sample structure. Two types of $In_{0.4}Ga_{0.6}As_{1-x}N_x$ QDs with nitrogen compositions of 0% and 2% were grown on GaAs(100) substrates by molecular-beam epitaxy using a radio frequency nitrogen plasma source. A nitrogen composition of 2% was roughly estimated by comparing the PL peak energy with the calculated transition energy (Fig. S1). The sample structure consists of a 400 nm-thick GaAs buffer, 5.5-ML-thick $In_{0.4}Ga_{0.6}As_{1-x}N_x$ QDs, a 10 nm-thick GaAs cap, a 30 nm-thick GaAs barrier, and 5.5-ML-thick $In_{0.4}Ga_{0.6}As_{1-x}N_x$ QDs. The surface QDs were grown under the same conditions as the buried QDs to observe their structures by atomic force microscopy (AFM). The growth temperature of the QDs and the cap layer was set to 753 K; the other layers were grown at 833 K. PL spectroscopy was performed in the temperature range of 4.5–400 K using a cooled InGaAs detector with a spectrometer. A continuous-wave laser or a mode-locked Ti:sapphire pulsed laser with a repetition rate of 80 MHz and a pulse width of <100 fs was used as the excitation source. The spot size of the excitation laser was approximately 0.05 mm. The laser energy was set to 1.55 eV for the excitation of the GaAs barrier. The laser power was varied from 0.01 to 3 mW. The time-resolved PL measurements were also performed from 4.5

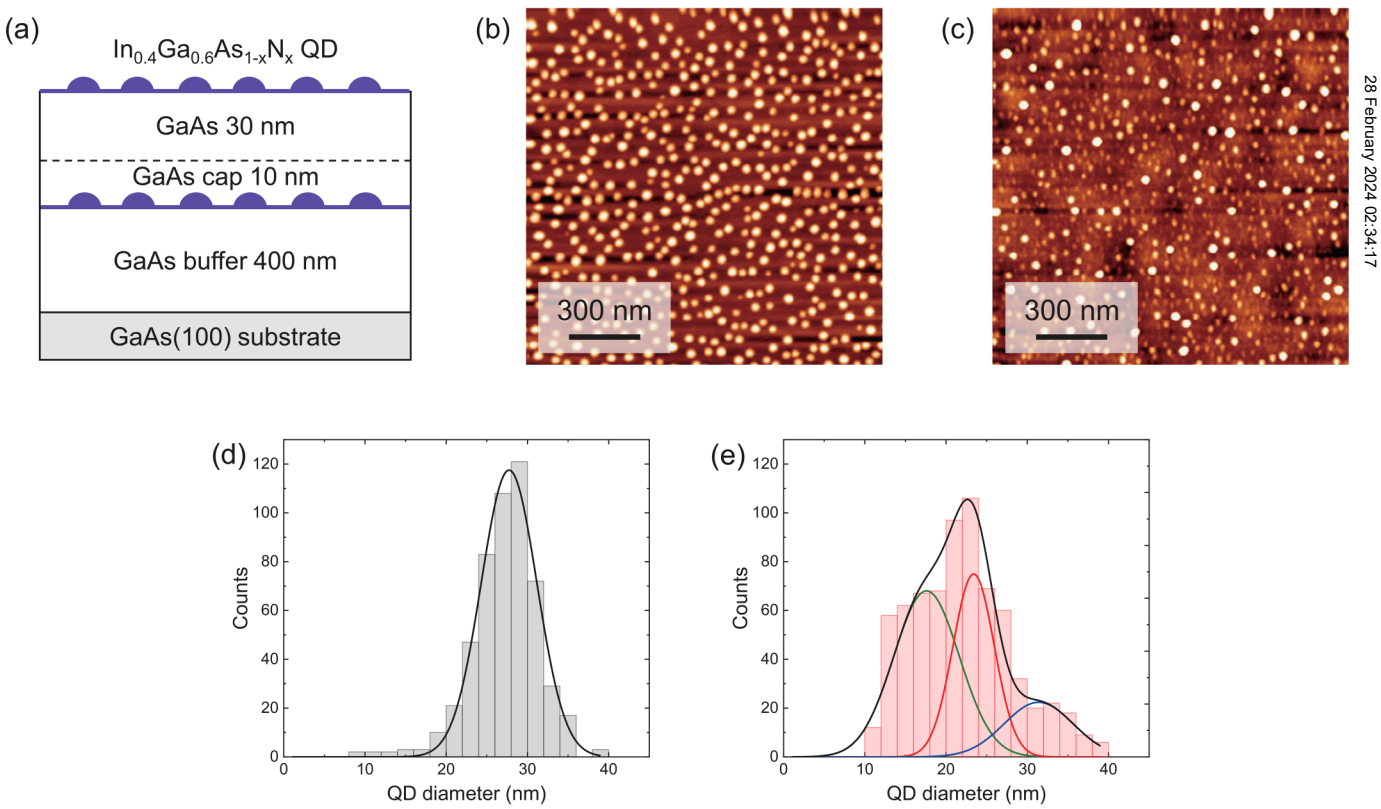

FIG. 1. (a) Schematic illustration of the sample structure. AFM images of (b) $In_{0.4}Ga_{0.6}As$ QDs and (c) $In_{0.4}Ga_{0.6}As_{0.98}N_{0.02}$ QDs. Distribution of the QD diameter of (d) $In_{0.4}Ga_{0.6}As$ QDs and (e) $In_{0.4}Ga_{0.6}As_{0.98}N_{0.02}$ QDs.

to 300 K at an excitation energy of 1.55 eV and an excitation power of 3 mW. The full width at half maximum (FWHM) of the laser-pulse time response curve was 14 ps.

III. RESULTS AND DISCUSSION

Figures 1(b) and 1(c) show the typical AFM images of the surfaces of $In_{0.4}Ga_{0.6}As$ QDs and $In_{0.4}Ga_{0.6}As_{0.98}N_{0.02}$ QDs, respectively. The AFM analysis revealed areal QD densities of 2.3×10^{10} and 3.2×10^{10} cm^{-2} for $In_{0.4}Ga_{0.6}As$ QDs and $In_{0.4}Ga_{0.6}As_{0.98}N_{0.02}$ QDs, respectively. Relatively homogeneous QDs can be observed in the $In_{0.4}Ga_{0.6}As$ QDs, whereas an inhomogeneous QD size is observed in the $In_{0.4}Ga_{0.6}As_{0.98}N_{0.02}$ QDs, in which small- and large-sized QDs coexist. This broad overview is clearly reflected in the size distribution of QDs. Figures 1(d) and 1(e) show the distribution of the QD diameter of $In_{0.4}Ga_{0.6}As$ QDs and $In_{0.4}Ga_{0.6}As_{0.98}N_{0.02}$ QDs, respectively. The averaged QD diameters were 27 and 22 nm for $In_{0.4}Ga_{0.6}As$ QDs and $In_{0.4}Ga_{0.6}As_{0.98}N_{0.02}$ QDs, respectively. The $In_{0.4}Ga_{0.6}As$ QDs exhibit a conventional Gaussian-like size distribution, whereas the size distribution of $In_{0.4}Ga_{0.6}As_{0.98}N_{0.02}$ QDs indicates the coexistence of small-sized QDs (18 nm), medium-sized QDs (23 nm), and large-sized QDs (31 nm). For both $In_{0.4}Ga_{0.6}As$ QDs and $In_{0.4}Ga_{0.6}As_{0.98}N_{0.02}$ QDs, the identical QD structures were observed not only in the different positions of the studied sample but also for the different samples grown under the same condition as in this study (Figs. S2 and S3). The inhomogeneity of dilute-nitride InGaAsN QDs has been previously observed.[25,32] This may be attributed to the formation of a rough wetting layer, which can be caused by inhomogeneous nitrogen incorporation or plasma damage.

Figure 2(a) shows the normalized PL spectra of the two samples at 4.5 K with a low excitation power of 0.01 mW. Each PL spectrum exhibits one major peak, which corresponds to the luminescence from the QD ground state. The PL peak energy significantly shifted from 1.27 to 1.15 eV with the addition of nitrogen. Because an increase in the nitrogen composition of InGaAsN reduces the bandgap energy, this result indicates nitrogen incorporation into the studied QDs. Further evidence for nitrogen in the QDs is discussed later. The broader PL spectrum of $In_{0.4}Ga_{0.6}As_{0.98}N_{0.02}$ QDs compared to that of $In_{0.4}Ga_{0.6}As$ QDs can be derived from the inhomogeneous size distribution of QDs, as described above. The PL spectrum of $In_{0.4}Ga_{0.6}As_{0.98}N_{0.02}$ QDs can be decomposed into three components with the peak energies of 1.07, 1.15, and 1.20 eV, as shown in Fig. 2(b). These PL emissions should originate from the different-sized QDs characterized by the AFM analysis, as discussed below.

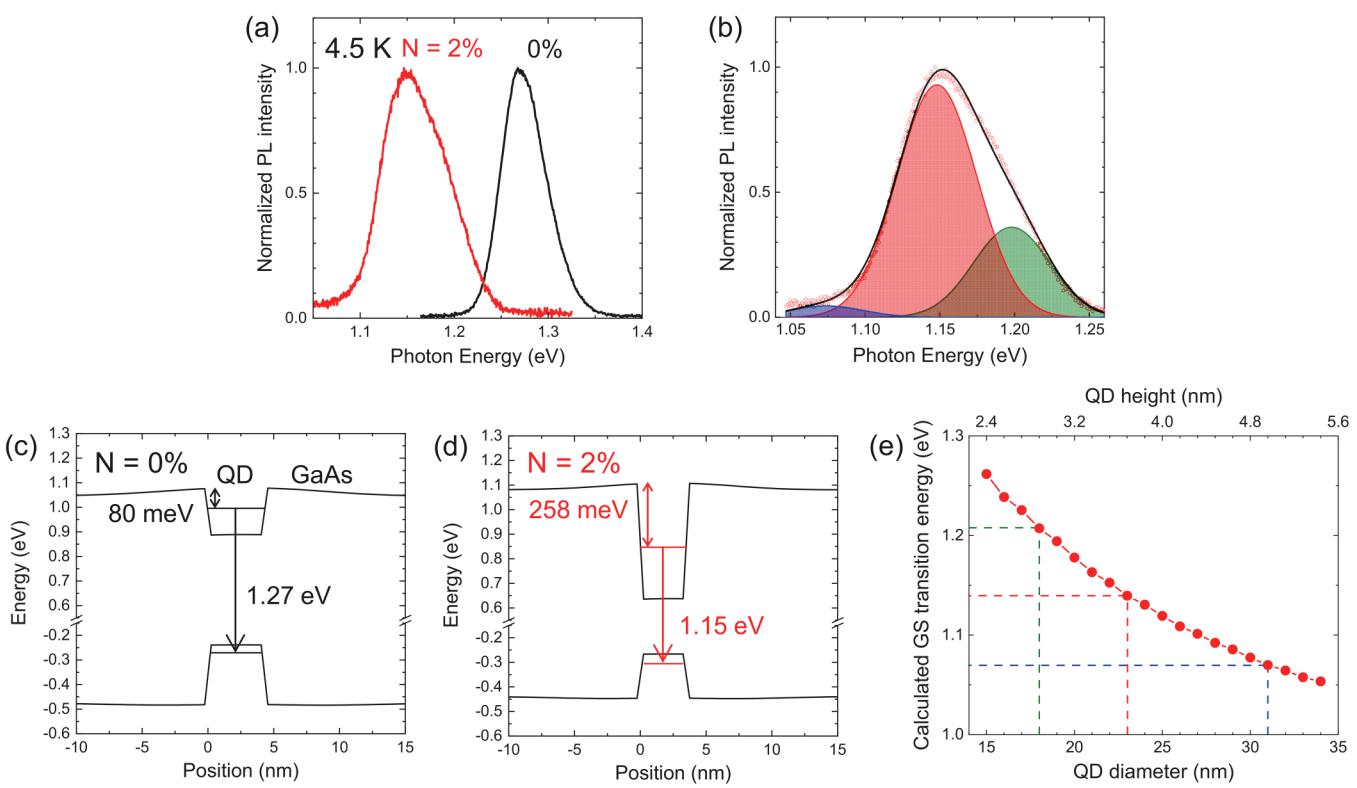

FIG. 2. (a) Normalized PL spectra of $In_{0.4}Ga_{0.6}As$ QDs and $In_{0.4}Ga_{0.6}As_{0.98}N_{0.02}$ QDs at 4.5 K. (b) Decomposition of the normalized PL spectrum of $In_{0.4}Ga_{0.6}As_{0.98}N_{0.02}$ QDs into three components. Three-dimensional calculated band profiles and ground states of (c) $In_{0.4}Ga_{0.6}As$ QDs and (d) $In_{0.4}Ga_{0.6}As_{0.98}N_{0.02}$ QDs. (e) Calculated ground-state (GS) transition energy of $In_{0.4}Ga_{0.6}As_{0.98}N_{0.02}$ QDs as a function of QD diameter (QD height) under the condition of the constant QD aspect ratio.

Figures 2(c) and 2(d) show the three-dimensional calculations of the band profiles and the ground states of the $In_{0.4}Ga_{0.6}As$ QDs and the $In_{0.4}Ga_{0.6}As_{0.98}N_{0.02}$ QDs, respectively. These calculations were performed at a lattice temperature of 4.5 K using the simulator nextnano.[38] We assumed truncated pyramidal QDs for the calculations of $In_{0.4}Ga_{0.6}As$ QDs and $In_{0.4}Ga_{0.6}As_{0.98}N_{0.02}$ QDs, with corresponding base sizes of 27 and 22 nm and heights of 4.3 and 3.5 nm, present on a 1 nm-thick wetting layer. These QD sizes were determined from the AFM analysis. The structural model and the QD aspect ratio were based on the scanning transmission electron microscopy of the reference $In_{0.4}Ga_{0.6}As$ QDs (Fig. S4), which differs from the sample investigated in this study. It is well known that the QD aspect ratio mainly depends on the growth temperature[39] and the growth rate[40] of the capping layer. These growth conditions of the GaAs capping layer were the same for two samples in this study, and thus, we assumed the same QD aspect ratio. This calculation also assumes uniform In and N compositions inside the QD and considers the influence of strain on the local band structure. The presence of strain increases the local band edge in the vicinity of the QDs.[41] The calculated transition energy of the QD ground state was 1.27 and 1.15 eV for the $In_{0.4}Ga_{0.6}As$ QDs and the $In_{0.4}Ga_{0.6}As_{0.98}N_{0.02}$ QDs, respectively. These values agree with the PL peak energies shown in Fig. 2(a). Notably, the incorporation of nitrogen into the $In_{0.4}Ga_{0.6}As$ QDs has a pronounced effect on the conduction band structure of the QDs. The calculated energy difference between the QD electron ground state and the GaAs barrier was 258 meV for the $In_{0.4}Ga_{0.6}As_{0.98}N_{0.02}$ QDs, which was higher than 80 meV of the $In_{0.4}Ga_{0.6}As$ QDs. The significantly larger barrier height suggests significant suppression of the thermal escape of electrons from the QDs, i.e., strong QD luminescence at and above room temperature.

Figure 2(e) shows the calculated ground-state (GS) transition energy of $In_{0.4}Ga_{0.6}As_{0.98}N_{0.02}$ QDs as a function of QD diameter (QD height) under the condition of the constant QD aspect ratio. As described above, the AFM analysis of $In_{0.4}Ga_{0.6}As_{0.98}N_{0.02}$ QDs indicates the coexistence of small-sized QDs (18 nm), medium-sized QDs (23 nm), and large-sized QDs (31 nm). Assuming that the buried QDs have the same distribution of the QD diameter as

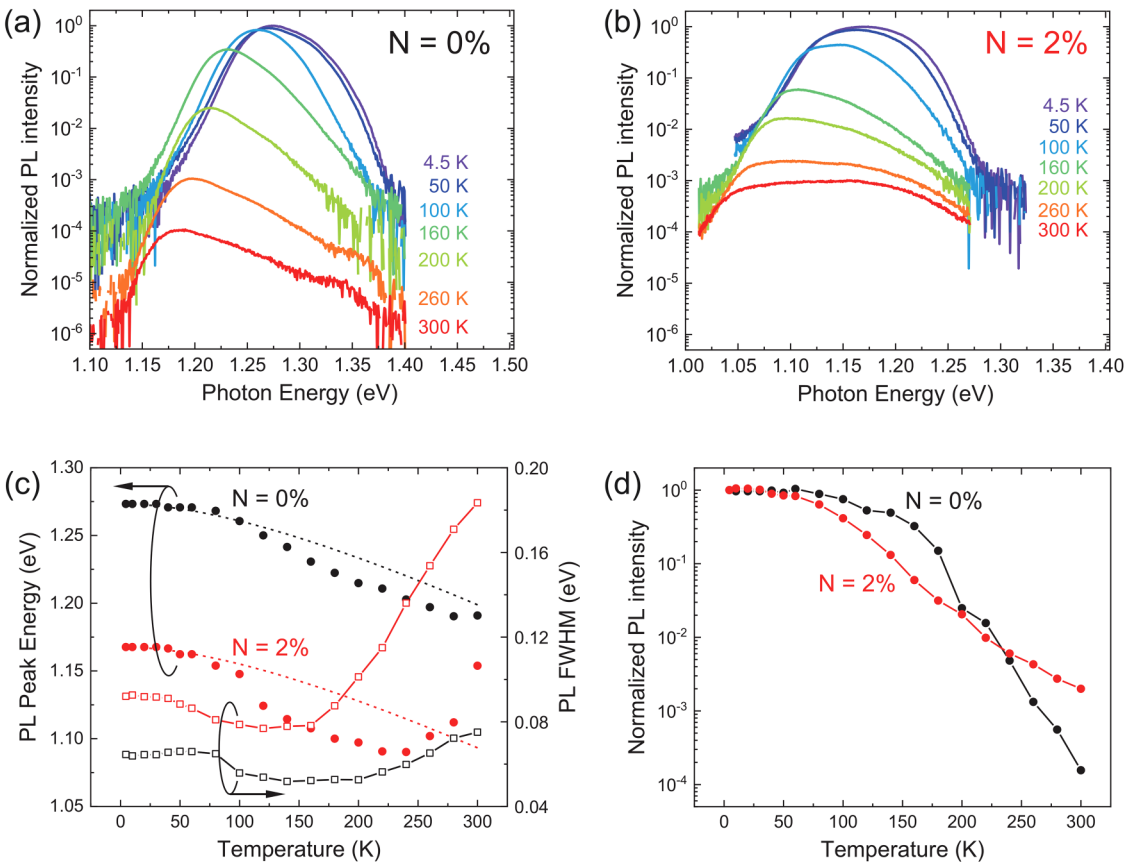

FIG. 3. PL spectra of (a) $In_{0.4}Ga_{0.6}As$ QDs and (b) $In_{0.4}Ga_{0.6}As_{0.98}N_{0.02}$ QDs measured at different temperatures. The PL intensities are normalized to the peak PL intensity at 4.5 K. Temperature dependence of (c) the PL peak energy and the PL FWHM and that of (d) the integrated QD PL intensity for $In_{0.4}Ga_{0.6}As$ QDs and $In_{0.4}Ga_{0.6}As_{0.98}N_{0.02}$ QDs. In (c), the dashed lines indicate Varshni fits to the closed circles from 4.5 to 100 K. In (d), the PL intensities are normalized to the PL intensity at 4.5 K for each sample.

the surface QDs, the ground-state transition energies of these different-sized QDs are estimated to be 1.21, 1.14, and 1.07 eV [see the dashed lines in Fig. 2(e)]. These values were in good agreement with the peak energies obtained by decomposing the PL spectrum [see Fig. 2(b)]. Although the buried QD structures of the studied samples were not directly observed in this work, the combination of PL analysis and three-dimensional band calculation suggests that the buried QDs have a distribution of the QD diameter comparable to that of the surface QDs.

Subsequently, we investigated the temperature dependence of the QD PL properties of each sample. Figures 3(a) and 3(b) show the PL spectra of $In_{0.4}Ga_{0.6}As$ QDs and $In_{0.4}Ga_{0.6}As_{0.98}N_{0.02}$ QDs, respectively, measured at different temperatures from 4.5 to 300 K. Here, the PL intensities were normalized to the peak PL intensity at 4.5 K. Significant differences were observed in the temperature evolution of the PL spectral shapes between the two samples. The PL peak energy and the PL full width at half maximum (FWHM) are shown in Fig. 3(c). At temperatures ranging from 100 to 200 K, the PL peak energies for both samples decreased with the temperature at a rate faster than that given by the Varshni fits obtained from 4.5 to 100 K. This fast redshift of the PL can be explained by the carrier transfer from smaller- to larger-sized QDs via the GaAs barrier or the wetting layer.[23,42] The larger redshift of the $In_{0.4}Ga_{0.6}As_{0.98}N_{0.02}$ QDs than that of $In_{0.4}Ga_{0.6}As$ QDs can be attributed to the inhomogeneous QD size distribution obtained by AFM. These results indicate that the PL spectra at high temperatures are dominated by the luminescence from the large-sized QDs.

At temperatures above 200 K, the decrease in the PL peak energy for the $In_{0.4}Ga_{0.6}As$ QDs became smaller, and the PL FWHM increased. This is mainly due to the thermal redistribution of carriers between the ground and excited states of the QDs. Note that significant increases in the PL peak energy and the PL FWHM were observed for the $In_{0.4}Ga_{0.6}As_{0.98}N_{0.02}$ QDs, indicating that the high-temperature luminescence originates from the ground and excited states. Generally, the energy difference between the QD electron excited states and the GaAs barrier is relatively small for InGaAs QDs; thus, the thermal redistribution of electrons from the excited states to the barrier can be dominant at high temperatures.[43] However, for InGaAsN QDs, significantly deeper electron potential can suppress the thermal escape of electrons from the QDs, as described above. Moreover, the resulting stronger localization of electrons in the QDs can increase the spatial overlap of the electron and hole wavefunctions, even at the excited states (Fig. S5). These two factors can enhance the luminescence efficiency of both the ground and excited states at high temperatures. The high luminescence efficiency of the $In_{0.4}Ga_{0.6}As_{0.98}N_{0.02}$ QDs is reflected in the temperature dependence of the PL intensity. Figure 3(d) shows the integrated QD PL intensity as a function of temperature for two samples. The PL intensity of the $In_{0.4}Ga_{0.6}As$ QDs decreased sharply above 160 K and subsequently decreased by three orders of magnitude at 300 K, whereas that of the $In_{0.4}Ga_{0.6}As_{0.98}N_{0.02}$ QDs decreased by only approximately one order of magnitude at temperatures ranging from 160 to 300 K. This result indicates the suppressed thermal escape of electrons from the QDs.

We next discuss the decrease in the PL intensity at temperatures above 160 K for the $In_{0.4}Ga_{0.6}As_{0.98}N_{0.02}$ QDs. Figure 4(a) shows the temperature dependence of the integrated PL intensity of the ground state in the temperature range of 50–300 K. Here, the QD ground state was defined as the energy range of 1.13–1.17 eV at 4.5 K. The energy range shifted with changing temperatures according to Varshni's law. The QD PL intensity is proportional to $\exp[E_a/kT]$, where E_a and k are the activation energy and the

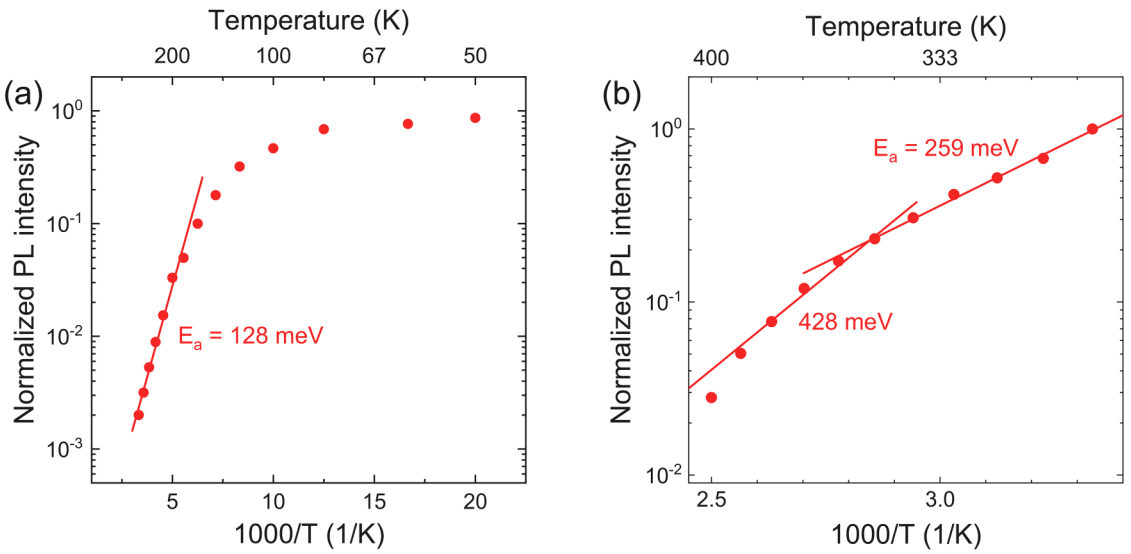

FIG. 4. Temperature dependence of the integrated PL intensity of the ground state in the temperature range of (a) 50–300 K and (b) 300–400 K for $In_{0.4}Ga_{0.6}As_{0.98}N_{0.02}$ QDs. The solid lines indicate the best-fitted results of thermal activation energies. In (a) and (b), the PL intensities are normalized to the PL intensity at 4.5 and 300 K.

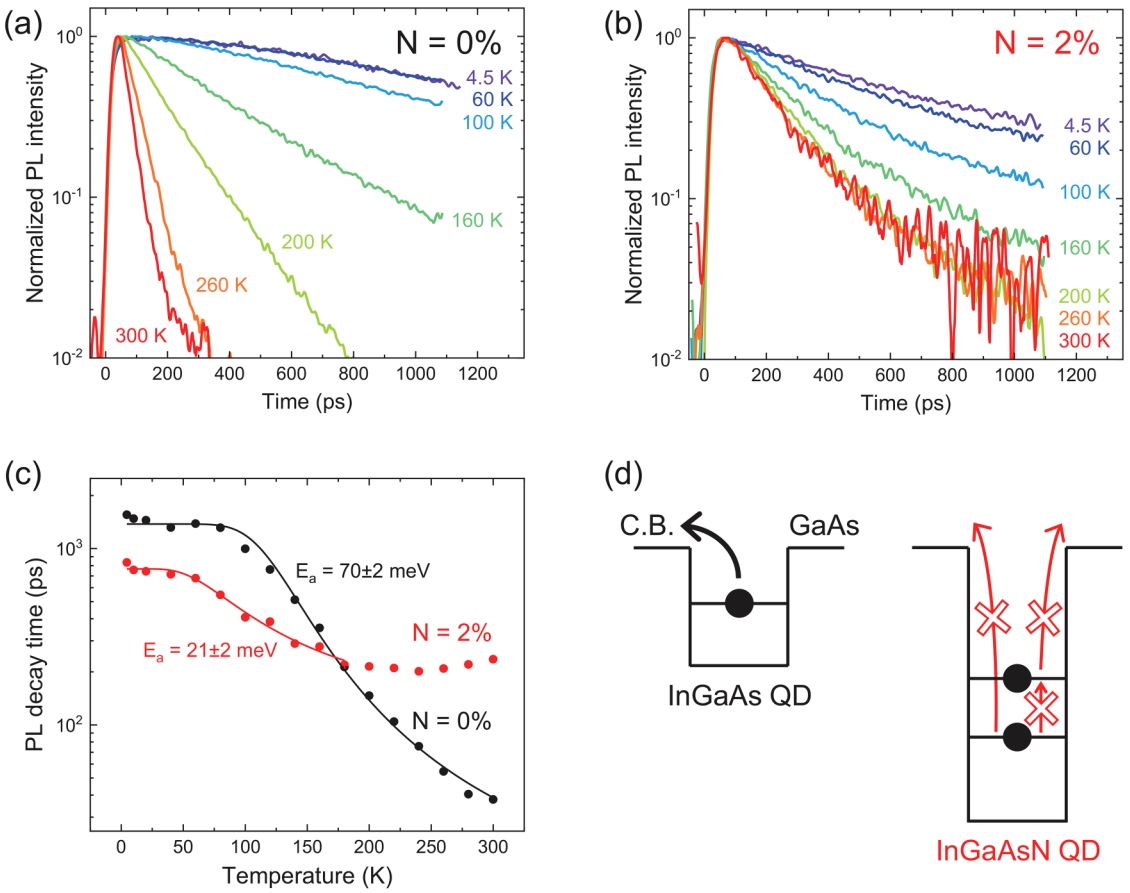

FIG. 5. Normalized PL decay curves of (a) $In_{0.4}Ga_{0.6}As$ QDs and (b) $In_{0.4}Ga_{0.6}As_{0.98}N_{0.02}$ QDs measured at different temperatures. (c) Temperature dependence of the PL decay time of $In_{0.4}Ga_{0.6}As$ QDs and $In_{0.4}Ga_{0.6}As_{0.98}N_{0.02}$ QDs in addition to Arrhenius fits (solid lines). (d) Schematic showing the significant suppression of the thermal escape and the thermal excitation of electrons in InGaAsN QD in comparison with InGaAs QD.

Boltzmann constant, respectively.[44] E_a can be obtained from the slope of the PL intensity. The best fitting gives $E_a = 128$ meV, as indicated in the solid line. This value was relatively close to the calculated hole confinement energy of 141 meV [Fig. 2(d)]. This result means that the decrease in the PL intensity at temperatures of 160–300 K can be due to the thermal escape of holes from the QDs, which demonstrates that the electron escape cannot be dominant in this temperature range. In contrast, other two activation energies are apparent at temperatures above 300 K, as shown in Fig. 4 (b). The measured activation energies of 259 and 428 meV were close to the calculated electron and exciton confinement energies of 258 and 399 meV [Fig. 2(d)]. Therefore, the decrease in the PL intensity above room temperature can be attributed to the electron escape or the exciton escape. Importantly, the good agreements between the measured activation energies and the calculated carrier confinement energies provide clear evidence for nitrogen in the QDs.

The temperature dependence of time-resolved PL was measured to further investigate the thermal carrier dynamics within the QDs. Figures 5(a) and 5(b) show the normalized PL decay curves of the ground states for the $In_{0.4}Ga_{0.6}As$ QDs and the $In_{0.4}Ga_{0.6}As_{0.98}N_{0.02}$ QDs, respectively, measured at different temperatures from 4.5 to 300 K. Here, the QD ground states of the $In_{0.4}Ga_{0.6}As$ QDs and the $In_{0.4}Ga_{0.6}As_{0.98}N_{0.02}$ QDs were defined as the energy ranges of 1.23–1.29 and 1.13–1.19 eV, respectively, at 4.5 K. The energy range shifted with changing temperatures according to Varshni's law. The PL decay time of the $In_{0.4}Ga_{0.6}As$ QDs rapidly decreased above 100 K, whereas the temperature dependence of the PL decay time of the $In_{0.4}Ga_{0.6}As_{0.98}N_{0.02}$ QDs was significantly smaller. The PL decay times of the two samples, obtained by single-exponential decay fitting, are shown in Fig. 5(c). For the $In_{0.4}Ga_{0.6}As$ QDs, the PL decay time decreased significantly from 1314 ps at 80 K to 38 ps at 300 K. The activation energy for the decrease in the PL decay time can be deduced as 70 ± 2 meV. This value is close to the calculated energy difference between the QD electron ground state and the GaAs barrier of 80 meV [Fig. 2(c)], demonstrating that the thermal escape of electrons from the QDs is dominant at 300 K for the $In_{0.4}Ga_{0.6}As$ QDs [Fig. 5(d)]. For the $In_{0.4}Ga_{0.6}As_{0.98}N_{0.02}$ QDs, the PL decay time decreased

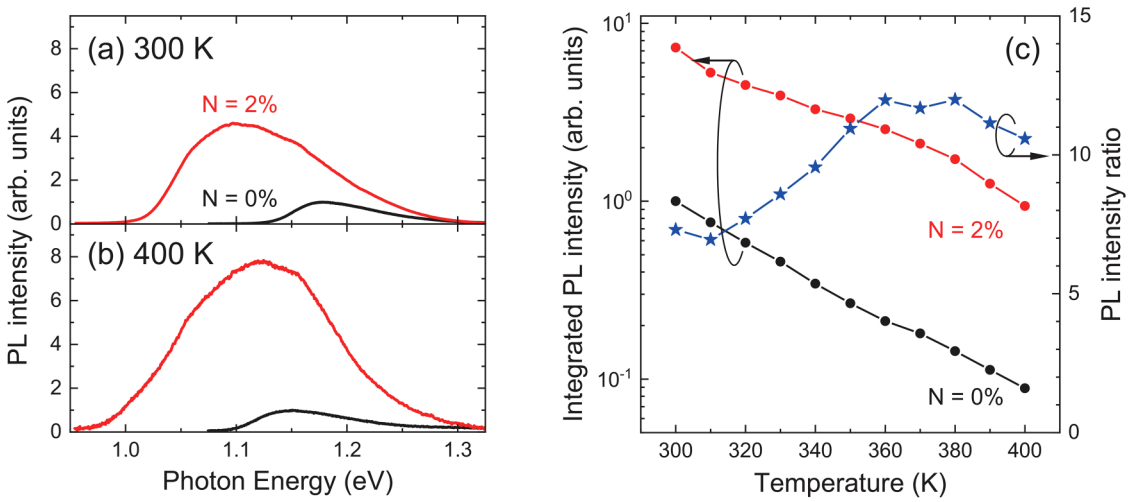

FIG. 6. PL spectra of $In_{0.4}Ga_{0.6}As$ QDs and $In_{0.4}Ga_{0.6}As_{0.98}N_{0.02}$ QDs at (a) 300 and (b) 400 K. The PL intensities are normalized to the peak PL intensity of $In_{0.4}Ga_{0.6}As$ QDs at each temperature. (c) Integrated PL intensity of $In_{0.4}Ga_{0.6}As$ QDs and $In_{0.4}Ga_{0.6}As_{0.98}N_{0.02}$ QDs as a function of temperature from 300 to 400 K and the corresponding PL intensity ratio.

from 834 ps at 4.5 K to 220 ps at 180 K, with an activation energy of 21 ± 2 meV. We anticipate that the activation energy is related to the nonradiative defects generated by the incorporation of nitrogen into the QDs. Note that the PL decay times of approximately 210 ps were almost constant at temperatures ranging from 180 to 300 K. This result demonstrates significant suppression of the thermal escape of electrons from the QDs and of the thermal excitation of electrons from the ground state to the excited state [Fig. 5(d)]. We expect that the suppressed thermal escape of electrons from the excited states can block the thermal excitation of electrons. By contrast, a significant decrease in the PL decay time with increasing temperature above 100 K was observed for the $In_{0.65}Ga_{0.35}As$ QDs with a higher In composition, which had emission energies similar to the studied $In_{0.4}Ga_{0.6}As_{0.98}N_{0.02}$ QDs (Fig. S6). Therefore, the temperature independence of the PL decay time in the high-temperature region was found to be unique to the dilute-nitride InGaAsN QDs with deep electron potential.

We discuss the effect of nitrogen incorporation on the QD PL intensity at and above room temperature from a practical perspective. Figures 6(a) and 6(b) show the PL spectra of the two samples at 300 and 400 K, respectively. The PL intensities were normalized to the peak PL intensity of the $In_{0.4}Ga_{0.6}As$ QDs at each temperature. When the temperature increased from 300 to 400 K, the PL peak energy of the $In_{0.4}Ga_{0.6}As$ QDs shifted to the lower energy with a decrease in the bandgap energy, whereas that of the $In_{0.4}Ga_{0.6}As_{0.98}N_{0.02}$ QDs shifted slightly toward higher energies. The higher-energy shift of the QD PL with increasing temperature should reflect the high luminescence efficiency of the QD excited states at high temperatures, which originates from both the suppressed thermal escape of electrons from the QD excited states and the large spatial overlap of the electron and hole wavefunctions at the excited states, as described above. The integrated QD PL intensities as a function of temperature from 300 to 400 K and the corresponding PL intensity ratios are shown in Fig. 6(c). The PL intensity ratio increased with increasing temperature, and the PL intensity of the $In_{0.4}Ga_{0.6}As_{0.98}N_{0.02}$ QDs at 400 K was one order of magnitude higher than that of the $In_{0.4}Ga_{0.6}As$ QDs. This result demonstrates that the thermal escape of electrons from the QDs can be suppressed in $In_{0.4}Ga_{0.6}As_{0.98}N_{0.02}$ QDs, even at a high temperature of 400 K, which is essential for industrial applications. As described above, the high-temperature PL is dominated by the luminescence from the large-sized QDs, particularly for the $In_{0.4}Ga_{0.6}As_{0.98}N_{0.02}$ QDs. In addition to the lowering of the QD conduction band by nitrogen incorporation, the improved carrier confinement for the large-sized QDs may contribute to the increased PL intensity at high temperatures. Stronger luminescence at high temperatures can be achieved by optimizing the nitrogen composition of InGaAsN QDs and determining the growth conditions that enable the growth of highly homogeneous QDs.

Finally, we compare our experimental results with a previous theoretical study of the electronic and optical properties of InGaAsN/GaAs QDs.[45] The previous study has shown that a substitutional 2% nitrogen addition to $In_{0.5}Ga_{0.5}As$ QDs causes lowering of the conduction band offset by about 200 meV, increasing the exciton binding energy of the ground state. The increase in the exciton binding energy may be reflected in our experimental result that the exciton escape becomes promoted at high temperatures above 350 K [Fig. 4(b)]. It is also predicted that the nitrogen addition to InGaAs QDs will improve the localization of the first and second excited states as well as the ground state. Therefore, we can conclude that our experimental findings of the high luminescence efficiency of the ground and excited states at high temperatures support well the previous theoretical study of InGaAsN/GaAs QDs.

IV. CONCLUSIONS

In summary, the temperature dependence of the PL properties of the $In_{0.4}Ga_{0.6}As_{0.98}N_{0.02}$ QDs was investigated by continuous-wave and time-resolved PL spectroscopy. We observed significant increases in the PL peak energy and the PL linewidth at temperatures above 200 K. This result indicates the high luminescence efficiency of both the QD ground state and the QD excited state at high temperatures owing to the deep electron potential of InGaAsN, in addition to the large spatial overlap of the electron and hole wavefunctions. The PL decay times were almost independent of the temperature above 200 K, with values of approximately 210 ps, indicating significant suppression of the thermal escape and the thermal excitation of electrons. Moreover, the PL intensity of the $In_{0.4}Ga_{0.6}As_{0.98}N_{0.02}$ QDs was one order of magnitude higher than that of the $In_{0.4}Ga_{0.6}As$ QDs at 400 K. These findings demonstrate that lowering the QD electron states can achieve strong QD luminescence above room temperature.

SUPPLEMENTARY MATERIAL

See the supplementary material for the calculated ground-state transition energy of the $In_{0.4}Ga_{0.6}As_{1-x}N_x$ QDs, the AFM analysis of $In_{0.4}Ga_{0.6}As$ QDs and $In_{0.4}Ga_{0.6}As_{0.98}N_{0.02}$ QDs, the high-angle annular dark-field scanning transmission electron microscopy of the reference $In_{0.4}Ga_{0.6}As$ QDs, spatial overlap integrals of the electron and hole wavefunctions of the $In_{0.4}Ga_{0.6}As_{1-x}N_x$ QDs, and the temperature dependence of the PL decay time for the $In_{0.65}Ga_{0.35}As$ QDs.

ACKNOWLEDGMENTS

This work was financially supported by JSPS KAKENHI (Grant Nos. JP16H06359, JP19K15380, JP20K20433, JP21H01356, and JP21KK0068), JST FOREST (Grant No. JPMJFR202E), Advanced Technology Institute Research Grants 2021, and the Murata Science Foundation.

AUTHOR DECLARATIONS

Conflict of Interest

The authors have no conflicts to disclose.

Author Contributions

Ayano Morita: Conceptualization (equal); Data curation (lead); Formal analysis (lead); Investigation (lead); Methodology (equal); Writing – original draft (lead). **Satoshi Hiura:** Conceptualization (lead); Formal analysis (equal); Funding acquisition (lead); Investigation (equal); Methodology (lead); Project administration (lead); Supervision (lead); Writing – review & editing (lead). **Junichi Takayama:** Data curation (supporting); Formal analysis (supporting); Investigation (supporting); Software (equal); Writing – review & editing (supporting). **Akihiro Murayama:** Conceptualization (equal); Funding acquisition (equal); Methodology (equal); Project administration (equal); Supervision (equal); Writing – review & editing (equal).

DATA AVAILABILITY

The data that support the findings of this study are available from the corresponding author upon reasonable request.

REFERENCES

[1]Y. Arakawa and H. Sakaki, Appl. Phys. Lett. **40**, 939 (1982).
[2]H. Saito, K. Nishi, I. Ogura, S. Sugou, and Y. Sugimoto, Appl. Phys. Lett. **69**, 3140 (1996).
[3]D. R. Matthews, H. D. Summers, P. M. Smowton, and M. Hopkinson, Appl. Phys. Lett. **81**, 4904 (2002).
[4]S. M. Kim, Y. Wang, M. Keever, and J. S. Harris, IEEE Photon. Technol. Lett. **16**, 377 (2004).
[5]M. G. Thompson, A. R. Rae, M. Xia, R. V. Penty, and I. H. White, IEEE J. Sel. Top. Quantum Electron. **15**, 661 (2009).
[6]S. Kim, H. Mohseni, M. Erdtmann, E. Michel, C. Jelen, and M. Razeghi, Appl. Phys. Lett. **73**, 963 (1998).
[7]S. J. Xu, S. J. Chua, T. Mei, X. C. Wang, X. H. Zhang, G. Karunasiri, W. J. Fan, C. H. Wang, J. Jiang, S. Wang, and X. G. Xie, Appl. Phys. Lett. **73**, 3153 (1998).
[8]H. Kamada, H. Gotoh, J. Temmyo, T. Takagahara, and H. Ando, Phys. Rev. Lett. **87**, 246401 (2001).
[9]A. Zrenner, E. Beham, S. Stufler, F. Findeis, M. Bichler, and G. Abstreiter, Nature **418**, 612 (2002).
[10]J. J. Finley, P. W. Fry, A. D. Ashmore, A. Lemaître, A. I. Tartakovskii, R. Oulton, D. J. Mowbray, M. S. Skolnick, M. Hopkinson, P. D. Buckle, and P. A. Maksym, Phys. Rev. B **63**, 161305 (2001).
[11]D. Regelman, E. Dekel, D. Gershoni, E. Ehrenfreund, A. Williamson, J. Shumway, A. Zunger, W. Schoenfeld, and P. Petroff, Phys. Rev. B **64**, 165301 (2001).
[12]G. S. Solomon, J. A. Trezza, A. F. Marshall, and J. S. Harris, Jr., Phys. Rev. Lett. **76**, 952 (1996).
[13]Z. R. Wasilewski, S. Fafard, and J. P. McCaffrey, J. Cryst. Growth **201–202**, 1131 (1999).
[14]F. Ferdos, S. Wang, Y. Wei, A. Larsson, M. Sadeghi, and Q. Zhao, Appl. Phys. Lett. **81**, 1195 (2002).
[15]Q. Gong, P. Offermans, R. Nötzel, P. M. Koenraad, and J. H. Wolter, Appl. Phys. Lett. **85**, 5697 (2004).
[16]H. Eisele, A. Lenz, R. Heitz, R. Timm, M. Dähne, Y. Temko, T. Suzuki, and K. Jacobi, J. Appl. Phys. **104**, 124301 (2008).
[17]T. Sugaya, T. Amano, M. Mori, and S. Niki, J. Vac. Sci. Technol. B **28**, C3C4 (2010).
[18]F. Heinrichsdorff, C. Ribbat, M. Grundmann, and D. Bimberg, Appl. Phys. Lett. **76**, 556 (2000).
[19]Z. Xu, D. Birkedal, M. Juhl, and J. M. Hvam, Appl. Phys. Lett. **85**, 3259 (2004).
[20]D. L. Huffaker, G. Park, Z. Zou, O. B. Shchekin, and D. G. Deppe, Appl. Phys. Lett. **73**, 2564 (1998).
[21]M. Sugawara, K. Mukai, and Y. Nakata, Appl. Phys. Lett. **74**, 1561 (1999).
[22]M. De Giorgi, C. Lingk, G. von Plessen, J. Feldmann, S. De Rinaldis, A. Passaseo, M. De Vittorio, R. Cingolani, and M. Lomascolo, Appl. Phys. Lett. **79**, 3968 (2001).
[23]S. Hiura, M. Takishita, J. Takayama, S. Sato, and A. Murayama, Phys. Rev. Appl. **14**, 044011 (2020).
[24]M. Kondow, K. Uomi, A. Niwa, T. Kitatani, S. Watahiki, and Y. Yazawa, Jpn. J. Appl. Phys. **35**, 1273 (1996).
[25]M. Sopanen, H. P. Xin, and C. W. Tu, Appl. Phys. Lett. **76**, 994 (2000).
[26]T. Hakkarainen, J. Toivonen, H. Koskenvaara, M. Sopanen, and H. Lipsanen, J. Phys.: Condens. Matter **16**, S3009 (2004).
[27]A. Nishikawa, R. Katayama, K. Onabe, Y. G. Hong, and C. W. Tu, J. Cryst. Growth **278**, 244 (2005).

[28]C. Y. Liu, S. F. Yoon, Z. Z. Sun, and K. C. Yew, Appl. Phys. Lett. **88**, 081105 (2006).
[29]H. Tsurusawa, A. Nishikawa, R. Katayama, and K. Onabe, Phys. Status Solidi B **243**, 1657 (2006).
[30]S. F. Yoon, C. Y. Liu, Z. Z. Sun, and K. C. Yew, Nanoscale Res. Lett. **1**, 20 (2006).
[31]S. Tomić, Appl. Phys. Lett. **90**, 25 (2007).
[32]M. J. Milla, A. Guzmán, R. Gargallo-Caballero, J. M. Ulloa, and A. Hierro, J. Cryst. Growth **323**, 215 (2011).
[33]Y. Huang, V. Polojärvi, S. Hiura, P. Höjer, A. Aho, R. Isoaho, T. Hakkarainen, M. Guina, S. Sato, J. Takayama, A. Murayama, I. A. Buyanova, and W. M. Chen, Nat. Photonics **15**, 475 (2021).
[34]K. Etou, S. Hiura, S. Park, J. Takayama, A. Subagyo, K. Sueoka, and A. Murayama, Phys. Rev. Appl. **19**, 024055 (2023).
[35]K. C. Yew, S. F. Yoon, Z. Z. Sun, and S. Z. Wang, J. Cryst. Growth **247**, 279 (2003).
[36]Z. F. Wei, S. J. Xu, and Q. Li, J. Appl. Phys. **100**, 124311 (2006).
[37]A. Nishikawa, Y. G. Hong, and C. W. Tu, J. Vac. Sci. Technol. B **22**, 1515 (2004).
[38]S. Birner, T. Zibold, T. Andlauer, T. Kubis, M. Sabathil, A. Trellakis, and P. Vogl, IEEE Trans. Electron Devices **54**, 2137 (2007).
[39]T. Kaizu, T. Matsumura, and T. Kita, J. Appl. Phys. **118**, 154301 (2015).
[40]A. D. Utrilla, D. F. Grossi, D. F. Reyes, A. Gonzalo, V. Braza, T. Ben, D. González, A. Guzman, A. Hierro, P. M. Koenraad, and J. M. Ulloa, Appl. Surf. Sci. **444**, 260 (2018).
[41]C. Pryor, Phys. Rev. B **57**, 7190 (1998).
[42]L. Brusaferri, S. Sanguinetti, E. Grilli, M. Guzzi, A. Bignazzi, F. Bogani, L. Carraresi, M. Colocci, A. Bosacchi, P. Frigeri, and S. Franchi, Appl. Phys. Lett. **69**, 3354 (1996).
[43]T. Yamamura, T. Kiba, X. Yang, J. Takayama, A. Subagyo, K. Sueoka, and A. Murayama, J. Appl. Phys. **116**, 094309 (2014).
[44]I. Ramiro, J. Villa, P. Lam, S. Hatch, J. Wu, E. Lopez, E. Antolin, H. Liu, A. Marti, and A. Luque, IEEE J. Photovolt. **5**, 840 (2015).
[45]S. Tomić, Phys. Rev. B **73**, 125348 (2006).